Analyzing the Dynamics of Lung Cancer Imaging Data Using Refined Fuzzy Entropy Methods by Extracting Different Features

LAL HUSSAIN[1], **WAJID AZIZ**[1,2], **ABDULRAHMAN A. ALSHDADI**[2],
MALIK SAJJAD AHMED NADEEM[1], **ISHTIAQ RASOOL KHAN**[2],
AND QURAT-UL-AIN CHAUDHRY[1]

[1]Department of Computer Science and IT, The University of Azad Jammu and Kashmir, City Campus, 13100 Muzaffarabad, Pakistan
[2]College of Computer Sciences and Engineering, University of Jeddah, Jeddah 23890, Saudi Arabia

Corresponding author: Qurat-Ul-Ain Chaudhry (annie.arshadch@gmail.com)

ABSTRACT Lung cancer is the major cause of cancer-related deaths worldwide with poor survival due to the poor diagnostic system at the advanced cancer stage. In the past, researchers developed computer-aided diagnosis (CAD) systems, which were greatly used by the radiologist for identifying the abnormalities and applied few features extracting methods. The physiology and behavior of various physiological systems can be best investigated using nonlinear dynamical measures for capturing the intrinsic dynamics, which is influenced due to multiple pathologies by the degradation of structural and functional components. As cancer images contain hidden information, which can be best analyzed using these dynamical measures. In this paper, we proposed multiscale sample entropy (MSE) with a mean and KD-tree algorithmic approach, multiscale permutation entropy (MPE), multiscale fuzzy entropy (MFE), and refined composite multiscale fuzzy entropy (RCMFE) with mean, variance, and standard deviation. The statistically significant results were computed to distinguish non-small-cell lung cancer (NSCLC) from SCLC by extracting morphological, texture, and elliptic Fourier descriptors (EFDs). The highest significant results obtained based on texture features using MFE with standard deviation give the P-value of 1.95E-50, morphological features using RCMFE with mean provide the P-value of 3.01E-14, and EFDs features using MFE with variance give the P-value of 1.04E-13. The results reveal that the improved complexity measures based on refined fuzzy entropy outperformed in analyzing the dynamics of lung cancer and will provide a new insight into extract meaningful hidden information present in the Lung cancer images, which will be very helpful to further distinguish NSCLC and SCLC for early diagnosis and prognosis.

INDEX TERMS Non small cell lung cancer (NSCLC), small cell lung cancer (SCLC), texture, morphological, multiscale fuzzy entropy (MFE), refined composite multiscale fuzzy entropy (RCMFE).

I. INTRODUCTION

The recent statistics of Lung cancer 2018 reveals that approximately 234,030 new cases of lung cancer are expected to be diagnosed and there would be 85% of whom will be non small cell lung cancer (NSCLC) [1], [2]. For detecting early NSCLC, there are two main approaches such as radiofrequency (RF) ablation and stereotactic body radiotherapy (SBRT). The two main types of Lung cancer are small cell lung carcinoma (SCLC) and non small cell lung carcinoma (NSCLC). Both of these types of lung cancer

have different ways of spreading and treatment. The cancer containing the features of both of these types is called mixed small cell/ large cell cancer. NSCLC is more common than SCLC which spread and grows very slowly. Where SCLC is related to smoking and grows very quickly and forms tumors and spread widely in the body. The deaths due to the lung cancer is related to the total amount of cigarette smoked [3].

Lung cancer is the most prevalent cancer and the leading cause of cancer-related deaths worldwide, resulting in more than 1.4 million deaths annually [4], [5]. Evaluation of the microscopic histopathology slides by experienced pathologists is indispensable to establish the diagnosis [6], [7] and defines the types and subtypes of lung cancers, including the

---

The associate editor coordinating the review of this manuscript and approving it for publication was Donatella Darsena.

two major types of non small cell lung cancer: adenocarcinoma and squamous cell carcinoma [8], [9].

SCLC is an aggressive form of lung cancer which is directly associated with the cigarette smoked. Its increasing evidences has implicated proto-oncogenes, autocrine growth loops, and tumor-suppressor genes in its development. Therefore, SCLC treatment and prognosis are different from NSCLC. An early detection of NSCLC can be helpful for survival rate of 35 to 85% depending upon the type and stage of tumor. As most of the cancer cases are detected late due to which the overall five-year survival rate for NSCLC is only 16%. Moreover, for SCLC standard therapy is chemotherapy which elicits a response in over 60% of SCLC patients. Therefore, the cancer returns within few months which result in an abysmal overall five-year survival rate of 6% for SCLC. These survival rates for both type of cancer have a little change for the past two decades.

The most common and frequently used imaging technique to diagnose the cancer is computed tomography (CT) [10]. The CT is one of the efficient technique used to diagnose the pulmonary nodules [11]. The structural and functional information about the human body is obtained using the X-rays. The CT image quality is influenced by the radiation dose. The performance of different machine learning algorithms that are useful to lung cancer prediction and prognosis are endeavored to explained and evaluated by [12]. It is proved that machine learning methods are commonly used to improve the performance or predictive accuracy of most prognosis, especially when compared to conventional statistical or expert-based systems. A survey of machine learning methods used in cancer prediction showing the types of cancer, clinical endpoints, choice of algorithm, performance and type of training data are discussed in detail. The following machine learning algorithm benefits and assumptions and limitations are discussed in method section: Decision Tree, Naïve Bayes, K-Nearest neighbor, Neural Network, Support Vector Machine (SVM) and Genetic Algorithm.

Data mining classification techniques on Lung cancer diagnosis are proposed by [13]. The Rule set classifier, Decision Tree, Neural Network and Bayesian Network classification algorithms are used for Lung Cancer analysis. From the result it was identified that Naïve Bayes algorithm produced better results than the other algorithms. Using fuzzy rules, [14] proposed a template matching technique based on genetic algorithms (GA) template matching (GATM) for detection of nodules existing within the lung area. In their work, GA was used to determine the target position in the observed image efficiently and to select an adequate template image from several reference patterns for quick template matching.

Computer-aided diagnosis (CAD) systems are efficient schemes that have been developed for the detection and characterization of various lesions in the field of the diagnosis of lung cancer. CAD system is mainly used for detection of lung cancer. The system deals with the problem of developing a computer based system for the extraction of maximum features from the segmented suspicious area from the lung X-ray image and these properties can be used to classify lung tumor as benign or malignant from the X-ray image directly [15].

Researchers in the past employed different features extracting strategies such as morphological, texture, scale invariant Fourier transform (SIFT), elliptic Fourier descriptors (EFDs), geometric, shape based features [16]–[21] for medical imaging problems. The existing techniques have some limitations as these methods are competitively expensive as most the important information is hidden in the cancer images in the region of interest which is of complex nature. Moreover, growth and proliferation of cancer cells also change the structural components thereby effecting the health of individuals and alter the complexity of the behavioral and physiological systems output. Thus, this problem can be more fully analyzed using the complexity based dynamical measures for further improving the detection performance. The physiological behavior of various physiological systems can be studied by examining the complexity of the systems [22]–[24] including behavior and physiological agin [25], [26], using nonlinear dynamical measures [27]–[30]. The complexity has been inherited with several other concepts such as randomness, entropy, and information theory [30]–[34]. Lipsitz [35] proposed the complexity reduced for control or physiological systems with aging disease. This reduction in complexity is due to the underlying structural or functional changes in the organization of the system. The behavior and physiological systems are influenced by multiple factors and their complexity is examined using several methods. Researchers computed various complexity-based methods such as approximate entropy [30], spectral analysis [36], Lyapunov exponent [37], detrended fluctuation analysis [38] to quantify the dynamics of various pathological systems. Hussain *et al.* [39], [40] recently employed MSE with KD tree algorithm and Refined Fuzzy entropy approaches in quantifying the dynamics of various physiological systems, the results obtained using these approaches outperformed than the traditional entropy methods.

II. MATERIAL AND METHODS
A. DATA SET
Datasets were taken from a publicly available database www.giveascan.org provided by Lung Cancer Alliance. The Lung Cancer Alliance (LCA) is the only national nonprofit organization providing patient support and advocacy exclusively to those living with or at risk for lung cancer and aim of this web-based repository is to facilitate in research purposes. Database Images are in Digital Imaging and Communications in Medicine (DICOM) format. This database comprises 76 patients with total of 945 images i.e. 568 from SCLC subjects and 377 from NSCLC subjects.

B. FEATURES EXTRACTION
For regression and classification, the most important step is to extract the most relevant feature. The detection performance

in machine learning classification problems is relying on the type of features extracted. In the past, researchers extracted different features e.g. hybrid features for detecting colon cancer [17]–[19]. Hussain et al. and co-workers recently extracted hybrid features based on texture, morphological, Scale invariant Fourier transform (SIFT), Elliptic Fourier descriptors (EFDs), entropy based complexity features for detecting prostate cancer, lung cancer, breast cancer and brain tumor [18], [20], [41]–[43]. Moreover, the complex dynamics of various physiological systems such as arrhythmia detection, epileptic seizure detection, Alzheimer disease, Alcoholism etc. [21], [40], [39], [44]–[49] have been studied. In this study, we first extracted morphological, texture and EFDs features and then employ the complexity measures to quantify the dynamics of lung cancer imaging data.

1) MORPHOLOGICAL FEATURES

The shape and structure characteristics of an image are determined using morphological features. In the past researchers used morphological features for computer-aided diagnostic systems. Researchers computed morphological features for automated prostate cancer localization [50], quantifying phenotypes for image analysis [51]–[53], detecting lung cancer [54], detection of seed of wild castor oil plants [55], colon cancer detection [18]. Recently Hussain et al. computed morphological features from prostate cancer images and computed the associations among these features to determine the strength between these features [56]. Morphological feature extraction module (FEM) takes input inside the shape of binary cluster and finds associated components in the clusters [57]. Researchers [18] in the past extracted nine morphological features which are: Perimeter (p), Eccentricity (y), location (a), Convex area (x), Euler quantity (l), Compactness (o), Orientation (e), duration of fundamental (m1), and Minor Axes (m2) are calculated for every issue of cluster. In this study, we extracted 14 different morphological features which are detailed and reflected in Figure 3 and Table 4 at Annex-A.

2) TEXTURE FEATURE

In previous studies, the texture features are most widely used in solving classification issues [58]–[60], particularly to classify the colon biopsie [61], [62], prostate cancer detection [20] and brain tumor detection [42]. Texture characteristics have been efficiently utilized in solving class related problems. The texture features are calculated from grey level cooccurrence matrix (GLCM) that covers the spatial relationship between pixels (of image). Each entry (u,v)th in the GLCM defines how frequently the pixel with intensity value u co-occur in a specified relationship with pixel having intensity value of v. The relationship between the pixels can be computed using (i) relative distance between neighboring pixels and pixels of interest and (ii) their orientation θ. Normally, the θ have four directions ($0^\circ 45^\circ 90^\circ 135^\circ$). There are fifteen features which can be obtained from GLCM including Entropy, Angular 2D moment, comparison,

correlation, nearby homogeneity, color, variance, common, Sum, prominence, difference entropy, sum entropy, distinction variance, sum variance, facts degree of correlation [63]. In this study, we extracted texture features which are reflected in Figure 3 and Table 5 at Annex-A.

3) ELLIPTIC FOURIER DESCRIPTORS (EFDs) FEATURE

To distinguish the elliptic shapes, the EFDs are most useful features. EFDs characteristics have been correctly used by many researchers for the characterization of closed shapes. Kuhl and Giardina [64] in 1982 introduced EFDs features to classify the solid objects such as box and car etc. Moreover, in pattern recognition systems [65], [66], EFDs features are most widely used. EFD method made up of an expansion of a shape as sum of ellipse. The Fourier Descriptors never change with translation of the shape and rotation. Two stages are required in computing EFDs features. In the first stage, the elliptic features are recognized in the white bunch of images. In the secondary phase, the elliptic object is arranged considering region along with EFDs of upper most N object be equal to the aimed Harmonic level Y. EFDs depend on chain codes by estimating the close shape by grouping of eight institutionalized line portions, are invariant to expansion, interpretation, rotation and beginning point of a closed shape. To obtain EFDs harmonic level Y, four coefficients i.e. t, u, v and w against every Harmonic level have computed detailed in [18], [20] as below:

$$t_i = [t_1 t_2 t_3, \ldots \ldots t_N] i^P \quad \text{Where } i = 1, 2, 3, \ldots N$$
$$u_i = [u_1 u_2 u_3, \ldots \ldots \ldots u_N] i^P$$
$$v_i = [v v_2 v_3, \ldots \ldots \ldots v_N] i^P$$
$$w_i = [w w_2 w_3, \ldots \ldots \ldots w_N] i^P \quad (1)$$

where $t_i u_i$, v_i and w_i vectors contain t, u, v and w Fourier coefficients of ith primitive up to harmonic level N. The average of these vectors is calculated as following: $\bar{t} = \frac{1}{N} \sum_{i=1}^{N} t_i$, $\bar{u} = \frac{1}{N} \sum_{i=1}^{N} u_i$, $\bar{v} = \frac{1}{N} \sum_{i=1}^{N} V_i$ and

$$\bar{w} = \frac{1}{N} \sum_{i=1}^{N} w_i \quad (2)$$

The Final elliptic feature vector (z) is determine by combining the above equation

$$z = [\bar{t}^P \bar{u}^P, \bar{v}^P, w^P]^P \quad (3)$$

The Fourier series f(x) is described by the equation:

$$f(x) = \frac{1}{2} n_0 + \sum_{a=1}^{\infty} [n_a \cos(nx) + m_a \sin(nx)] \quad (4)$$

The elliptic Fourier coefficients of the n-th harmonic (an, bn, cn, dn) detailed in [67] are given as:

$$a_n = \frac{T}{2n^2\pi^2} \sum_{p=1}^{k} \frac{\Delta x_p}{\Delta t_p} \left[\cos\left(\frac{2n\pi t_p}{T}\right) \right.$$
$$\left. - \cos\left(\frac{2n\pi t_{p-1}}{T}\right) \right] \quad (5)$$

$$b_n = \frac{T}{2n^2\pi^2} \sum_{p=1}^{k} \frac{\Delta x_p}{\Delta t_p} \left[\sin\left(\frac{2n\pi t_p}{T}\right) \right.$$
$$\left. - \sin\left(\frac{2n\pi t_{p-1}}{T}\right) \right] \qquad (6)$$

$$c_n = \frac{T}{2n^2\pi^2} \sum_{p=1}^{k} \frac{\Delta y_p}{\Delta t_p} \left[\cos\left(\frac{2n\pi t_p}{T}\right) \right.$$
$$\left. - \cos\left(\frac{2n\pi t_{p-1}}{T}\right) \right] \qquad (7)$$

$$d_n = \frac{T}{2n^2\pi^2} \sum_{p=1}^{k} \frac{\Delta y_p}{\Delta t_p} \left[\sin\left(\frac{2n\pi t_p}{T}\right) \right.$$
$$\left. - \sin\left(\frac{2n\pi t_{p-1}}{T}\right) \right] \qquad (8)$$

T is the period (the interval), n is the number of the harmonic, p is the index of the chain link, k is the number of chain links, and tp and tp-1 are the lengths of the chain at the pth link.

The truncated Fourier approximation to a closed contour can be written as:

$$x(t) = A_0 + \sum_{n=1}^{N} X_n \qquad (9)$$

$$y(t) = C_0 + \sum_{n=1}^{N} Y_n \qquad (10)$$

where components of projections X_n and $Y_n (1 \leq n \leq N)$ are

$$X_n(t) = a_n \cos\frac{2\pi nt}{T} + b_n \sin\frac{2\pi nt}{T} \qquad (11)$$

$$Y_n(t) = c_n \cos\frac{2\pi nt}{T} + d_n \sin\frac{2\pi nt}{T} \qquad (12)$$

And A_0 and C_0 are the DC components of the Fourier series.

The contours are chain-coded represented by x and y coordinates of ordered points. Consider contour between the (i-1)th and ith chain-coded point is linearly interpolated and contour length from starting point to the pth point and perimeter to the contour are represented by tp and T respectively, then

$$t_p = \sum_{i=1}^{p} \Delta t_i \qquad (13)$$

where Δt_i is the distance between (i-1)th and ith point.

The x and y coordinates of pth points are:

$$x_p = \sum_{i=1}^{p} \Delta x_i \qquad (14)$$

$$y_p = \sum_{i=1}^{p} \Delta y_i \qquad (15)$$

where Δx_i and Δy_i are the distance along x and y axis between (i-1)th and ith points. Thus, elliptic Fourier expansion of the coordinates on the contour are given by:

$$x_p = A_0 + \sum_{n=1}^{\infty} \left(a_n \cos\left(\frac{2n\pi t_p}{T}\right) + b_n \sin\left(\frac{2n\pi t_p}{T}\right) \right) \qquad (16)$$

$$y_p = C_0 + \sum_{n=1}^{\infty} \left(c_n \cos\left(\frac{2n\pi t_p}{T}\right) + d_n \sin\left(\frac{2n\pi t_p}{T}\right) \right) \qquad (17)$$

The Fourier series describe by the above equation approximates the true function arbitrarily well on any finite interval. If one replaces the infinite sum with a finite one, from n = 1 to k, this is called the kth harmonic; the higher the value of k, the better the approximation.

In order to modify ellipse to approximate the closed contour, below is the equation that gives the nth Elliptic Fourier Descriptor.

$$\frac{(d_n^2 + c_n^2)X_n^2 + (a_n^2 + b_n^2)Y_n^2 - 2X_nY_n(a_nc_n + b_nd_n)}{(a_nd_n - b_nc_n)} = 1 \qquad (18)$$

C. NONLINEAR DYNAMICAL ANALYSIS
In the present study, we extracted morphological, texture and EFDs features from lung cancer images and then apply the following complexity-based approaches to quantify the dynamics of lung cancer images.

1) REFINED MULTISCALE FUZZY ENTROPY
Entropy is broadly used to measures what has been generally utilized in physiological signal examination. One of the mostly used entropy-based methodologies is sample entropy, which is relatively robust to noise and the other extensively used entropy method is fuzzy entropy. Recently, these two techniques have most widely used in many applications. In spite of the fact that sample entropy is slightly faster than fuzzy entropy, however, later is more stable to the data length [40], [68], [69].

In fuzzy entropy, for the time series $x = (x_1, x_2, \ldots x_n)$, embedding dimension h, and tolerance t, $S_r^h = \{x_r, x_{r+1}, \ldots x_{r+h-1}\} - x0_r$ is formed where $x0_r = \sum_{j=0}^{h-1} \frac{x_{t+j}}{h}$, the distance between each of S_{r1}^h and S_{r2}^h is defined as: $d_{ri,r2} = d\left[S_{r1}^h, S_{r2}^h\right] = \max[|S_{r1+m}^h - S_{r2+m}^h| : 0 \leq h \leq r - 1$ and $r_1 \neq r_2]$.

For Fuzzy entropy the power and tolerance are denoted as n and t, the similarity amount $d_{ri,r2}$ is computed through a fuzzy function $\mu(d_{rir2}, n, t)$ as $\exp\left(-(d_{ri,r2})^n/t\right)$ the function α^h is defined as:

$$\alpha^h(x,n,t) = \frac{1}{N-h} \sum_{r1=1}^{N-h} \frac{1}{N-h-1} \sum_{r2=1, r1 \neq r2}^{N-m} \exp\left(-(d_{ri,r2})^n/t\right) \qquad (19)$$

Finally, the Fuzzy entropy of the signal is computed as the negative natural logarithm of the ratio of α^h and α^{h+1}.

$$FE(x, h, n, t) = -\ln\left(\alpha^{h+1}/\alpha^h\right) \qquad (20)$$

The complication of a system can be calculated with numerous nonlinear dynamical procedures such as entropy related techniques. These techniques are used to identify the healthy and non-healthy groups to quantity the complexity of the biological actions.

2) MULTISCALE SAMPLE ENTROPY (MSE)

In the past, researchers quantified the complex dynamics of physiological and neurophysiological signals by applying entropy measures. One of the most popular time series is sample entropy which is computed as an unbiased estimator of the conditional probability that two timeseries with m consecutive points will remain similar when there is one or more consecutive points are added (where m denotes the embedding dimension). Sample entropy was derived from the developed approaches of Grassberger and co-workers [70]–[73].

Sample entropy was used to mine information in a time sequence and measurements of the organized structure was agreed by testing the repeated patterns of varying length. It is calculated as a negative average natural logarithm of conditional probability.

Consider a time sequences a (1), a (2), a (3), a (4)...a (N), where N is the data length. Sample entropy can be calculated as follow:

$$A (i) = A (i), A(i + 1), A(i + 2) \ldots (Ai + m-1)]. \quad (21)$$

where $i = 1, 2, 3 \ldots N - m + 1$.

The distance d [A(i), A(j)] between two series A(i) and A(j) is calculated as:

$$[A (i), A (j)] = \max[|a(i + r) - -a(j + r)|] \quad (11)$$

where $r = 0, 1, 2 \ldots m - 1$.

And $j = 1, 2, 3 \ldots N - m + 1$; but $j \neq i$.

Count d [A (i), A (j)] which is smaller than the given threshold, then calculated the ratio of this number with total $N - m$ as

$$R_i^m (s) = \frac{\{number \ of \ d \left[A (i) , A (j) \right] < s\}}{N - m} \quad (22)$$

Compute $R_i^m (s)$ for all I as:

$$R^m (s) = \frac{\sum R_i^m (s)}{N - m + 1} \quad (23)$$

In order to obtain increment in dimension, increase one to number of dimensions of the vector. Repeat the above steps I to IV until $R^{m+1} (s)$ is obtained.

The sample entropy is calculated as:

$$SamEN (N, s, m) = - \ln \left[\frac{R^{m+1} (s)}{R^m (s)} \right] = \ln \frac{w_d}{w_n} \quad (24)$$

As discussed earlier, Sample entropy methods provide limited performance for complex data, and is not appropriate for a complex time sequences whose features are calculated at various scales. MSE is calculated at numerous time scales. It has been established using coarse grained time series.

For a one-dimensional time series,

$$u = \{u_1, u_2, u_3, \ldots u_n\}$$

The following equation calculate the coarse-grained time sequences f (τ) at scale τ

$$f_a^\tau = \frac{1}{\tau} \sum_{b=(a-1)\tau+1}^{a\tau} u_b, \quad 1 \leq a \leq \frac{N}{\tau} \quad (25)$$

3) SAMPLE ENTROPY WITH K-D TREE ALGORITHMIC APPROACH

The sample entropy was proposed by [74] is a modified form of approximate entropy. The sample entropy in comparison to approximate entropy shows good features line trouble free implementation and independent of data length. Manis (2008) [75] proposed K-D tree algorithmic approach using approximate entropy. An improved version of K-D tree algorithm was proposed by [76] that can create the multiple randomized K-d trees. Pan *et al.* (2011) [77] developed new K-d tree algorithm based on sample entropy detailed in [39], which is more efficient with respect to performance, space and time complexity using following steps:

Step 1. Transform the original discrete time series to a special point set from $x = \{x1, x2, x3, \ldots .xN$

Step 2. The d-dimensional K-d tree is constructed using N-m points for which total cost is O (N long N) and memory is O(N)

Step 3. Range query; For, d-dimensional K-d tree search the time cost is $NO(N^{1\frac{1}{d}})$ for N queries and memory cost is O(N)

4) MULTISCALE PERMUTATION ENTROPY (MPE)

Permutation entropy states the local order structure of the time series, which can give a computable complexity measure for a dynamical time series. Permutation entropy was presented as a computational proficient technique for extracting the data from complex framework. At each time's' of a given a time series [78].

$$A = (a_1 + a_2 + a_3 \ldots .a_n) \quad (26)$$

A vector collected as the mth preceding values is formed:

$$U \rightarrow \left(A_\tau, A_{\tau+1}, \ldots .A_{\tau+(p-2)}, A_{\tau+(p-1)} \right) \quad (27)$$

where p is called embedding dimension and represent how information is present in a vector and τ is time delay. For a given embedding dimension there will be p! Possible permutation p.

Permutation entropy follows the concept of Shannon entropy by examining the relative frequency of patterns generated form time series. The permutation entropy (PE) is defined as:

$$PerEn = - \sum_{i=1}^{p} \pi_i \ln \pi_i \quad (28)$$
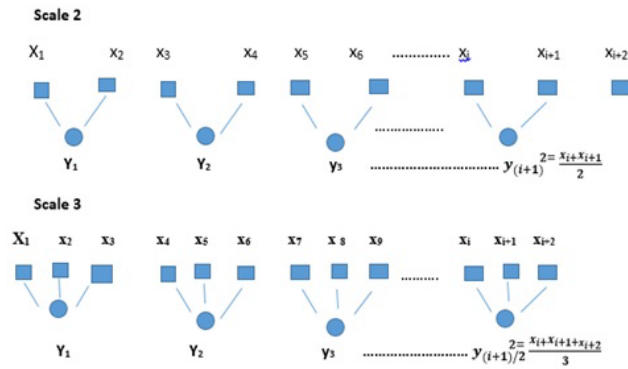
FIGURE 1. Coarse grained time series procedure.

FIGURE 2. SCLC and NSCLC.

Permutation entropy depends on the choice of embedding dimension 'p' and time delay 'τ'. [79] recommended that value of embedding dimension 'p' should be $3 \leq p \leq 7$ and time delay $\tau = 1$. Normalized permutation entropy is calculated by the following formula:

$$NPerEn = -\frac{PerEn}{\ln p!} \tag{29}$$

where $\ln p!$ represents extreme PE value.

MPE incorporates two procedures [80] First, a coarse-graining process detailed in [44] is applied to a time series as reflected in the Figure 1. For a given time series $(a_1, a_2, a_3 \ldots .a_n)$, a repeated coarse-grained time series is formed by averaging a successively increasing number of data points in non-overlapping windows. Each element of a multiple coarse-grained time series m_j^v is computed as:

$$m_j^v = 1/v \sum_{i=(j-1)v+1}^{jv} a_i \tag{30}$$

v defines the scale factor and $1 \leq j \leq L/v$. The coarse-grained time series is simply the original time series when $v = 1$.

Now, PE is computed for each coarse-grained time series and plotted as a function of the scale factor v. To calculate the permutation of a coarse-grained time series $w_j, v_t = \left[w_t, w_{t+1}, \ldots., w_{t+p-1} \right]$ is created with the embedding p and then organized in an increasing order: $w_{t+j_1-1} \leq w_{t+j_2-1}, \ldots. \leq w_{t+j_n-1}$. There are p! Possible patterns, called permutations.

Let f(x) defines the frequency in the time series, its relative frequency is:

$$R(x) = \frac{f(x)}{L/v^- p + 1} \tag{31}$$

The permutation entropy is computed as follow:

$$PerEn = -\sum_{i=1}^{p} p(\pi_i) \ln p(\pi_i) \tag{32}$$
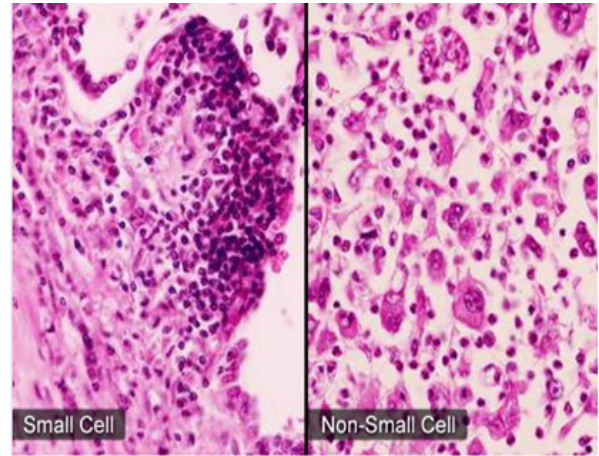
If the value of PE = 1 than all permutations have an equal chance to occur and if the PE = 0 then it shows that the time series is regular.

III. RESULTS
In this study, we first extracted texture, morphological and EFDs features from Lung cancer images then applied the entropy-based complexity measures such as Multiscale sample entropy (MSE), multiscale permutation entropy (MPE), Multiscale sample entropy based on KD-tree algorithmic approach, Multiscale Fuzzy entropy (MFE) based on mean, variance and standard deviation, refined composite Multiscale Fuzzy entropy (RCMFE) based on mean, variance and standard deviation.

In Table 1, KD- Tree algorithm was employed to distinguish SCLC group with NSCLC using different features which include morphological, texture, and EFD. The most significant result using KD Tree algorithm for morphological features were obtained at scale 1 having minimum P-value = 4.43E-11 with mean $\pm$ SD = 0.2749 $\pm$ 0.1453 for NSCLC and mean $\pm$ SD = 0.2179 $\pm$ 0.0768 for SCLC and is more significant with other values. For texture features we get most significant result at scale 3 having P-value = 3.51E-24 with mean $\pm$ SD = 0 $\pm$ 0 for NSCLC and mean $\pm$ SD = 0.3638 $\pm$ 0.5112 for SCLC and is more significant with other values. At scale 5, 6, 7 no P- value appear shows no separation between groups. Similarly, for EFD features, we obtained most significant result at scale 7 having P- value = 2.06E-06 with mean $\pm$ SD = 0.6413 $\pm$ 0.5393 for NSCLC and mean $\pm$ SD = 0.8532 $\pm$ 0.4637 for SCLC and is more significant with other values, respectively using K-D tree algorithmic approach as reflected in Table 3.

If we compare mean value of both classes using Morphological feature NSCLC exhibit higher complexity than SCLC subjects. As reflected in Table 3, by employing Multiscale sample entropy (MSE) and extracting morphological features, the NSCLC (0.4050) exhibit higher complexity than SCLC (0.3397). Similarly, by employing MSE

TABLE 1. Distinguishing NSCLC and SCLC group using KD –tree algorithm for morphological, texture and EFD features.

Scale	MSE with KD tree algorithmic approach								
	Morphological features			Texture features			EFDs features		
	NSCLC	SCLC	P-value	NSCLC	SCLC	P-value	NSCLC	SCLC	P-value
	Mean ± SD	Mean ± SD		Mean ± SD	Mean ± SD		Mean ± SD	Mean ± SD	
1	0.2749 ± 0.1453	0.2179 ± 0.0768	4.43E-11	0.2007 ± 4.7279E-16	0.2007 ± 4.7279E-16	-	1.0828 ± 0.8578	1.3950 ± 0.7179	8.88E-05
2	0.2742 ± 0.1454	0.2277 ± 0.0923	8.09E-08	0.1016 ± 0.3660	0.4348 ±0.5352	6.21E-16	1.0509 ± 0.8748	1.3386 ± 0.7725	8.16E-05
3	0.2895 ± 0.1550	0.2496 ± 0.1179	3.52E-05	0 ± 0	0.3638 ± 0.5112	3.51E-24	1.0354 ± 0.8817	1.3331 ±0.7796	7.92E-05
4	0.3233 ± 0.1680	0.2815 ± 0.1413	1.40E-04	0 ± 0	0.1857 ± 0.3963	1.24E-12	1.0459± 0.8772	1.3442 ± 0.7678	6.16E-05

TABLE 2. Distinguishing NSCLC and SCLC group using MFE (variance) entropy for morphological, texture and EFD features.

Scale	MFE with variance								
	Morphological features			Texture features			EFDs features		
	NSCLC	SCLC	P-value	NSCLC	SCLC	P-value	NSCLC	SCLC	P-value
	Mean ± SD	Mean ± SD		Mean ± SD	Mean ± SD		Mean ± SD	Mean ± SD	
2	0.1641 ± 0.5056	0.0029 ± 0.0291	2.55E-12	-0.9163 ± 1.1292 E-07	-0.9163 ± 4.2841E-06	4.19E-40	-6.4950 ± 5.2877	-4.3074 ± 2.0975	2.94E-10
3	3.1974E-04 ± 9.9734E-04	0 ± 0	3.03E-07	-0.4055 ± 1.7035 E-07	-0.4055 ± 6.2920E-06	3.25E-36	-1.5283 ± 3.7878	-2.1017 ± 3.5686	5.80E-06
4	-	-	-	1.0624 E-07 ± 3.6932 E-07	3.9849E-06 ± 8.5656E-06	4.30E-33	0.2180 ± 2.1232	0.0522 ± 1.4439	2.16E-01
5	-	-	-	-	-	-	2.1503 ± 4.3693	0.0920 ± 0.6323	1.04E-13

and computing texture features a higher complexity of NSCLC (1.7964) than SCLC (1.5720). Moreover, NSCLE (2.0266) exhibit higher complexity than SCLC (1.8460) by extracting EFDs features and applying MSE. These findings are consistent with the previous studies [81]–[85] and [39], [44], [45], [48].

In Table 2, MFE based on variance was employed to distinguish SCLC group from NSCLC. We got most significant result at scale 2 for morphological feature having P-value (2.55E-12) with mean ± SD = 0.1641 ± 0.5056 for NSCLC and mean ± SD = 0.0029 ± 0.0291 for SCLC. Similarly, we get significant result for Texture feature at scale 2 having

TABLE 3. Distinguishing NSCLC and SCLC group using different entropy measures reflecting only optimal results based on morphological, texture and EFD features.

Scale	Multiscale Sample entropy								
	Morphological features			Texture features			EFDs features		
	NSCLC	SCLC	P-value	NSCLC	SCLC	P-value	NSCLC	SCLC	P-value
	Mean ± SD	Mean ± SD		Mean ± SD	Mean ± SD		Mean ± SD	Mean ± SD	
2	0.4050± 0.149	0.3397± 0.036	5.21E-11	1.7964 ± 0.677	1.572 ± 0.553	5.48E-07	2.0266 ± 0.416	1.846± 0.2001	4.08E-07
	Multiscale Permutation Entropy								
2,1,1	1.373 ± 0.064	1.386± 2.66E-15	2.50E-03	2.151± 0.114	2.1800± 0.066	7.58E-04	2.218 ± 0.192	2.112 ± 0.108	3.78E-12
	MSE using KD-tree Algorithmic approach								
1, 2,7	0.275 ± 0.145	0.218 ± 0.076	4.43E-11	0.102 ± 0.366	0.434 ±0.535	6.21E-16	0.641 ± 0.539	0.853 ± 0.464	2.06E-06
	MFE (Mean)								
1, 1,5	0.082±0.085	0.107± 0.042	3.01E-14	-1.610± 0.002	-1.618 ± 0.011	9.81E-34	1.502± 1.309	2.021± 0.809	2.46E-09
	MFE (Variance)								
2,3,5	0.164 ± 0.506	0.003 ± 0.029	2.55E-12	-0.406 ± 1.703E-07	-0.406± 6.292E-06	3.25E-36	2.150 ± 4.369	0.092 ± 0.632	1.04E-13
	MFE (SD)								
2,2,2	0.238 ± 0.649	0.014± 0.039	1.16E-10	-0.916 ± 1.541E-04	-0.915± 0.001	1.95E-50	0.554 ± 1.100	0.049 ± 0.262	1.82E-12
	RCMFE (Mean)								
1,1,2	0.0820 ± 0.1065	0.0297 ± 0.0420	3.01E-14	-1.6104 ± 0.0019	1.6183 ± 0.0106	9.81E-34	-2.1451 ± 1.3111	-2.6228 ± 0.7580	3.89E-05
	RCMFE (Variance)								
2, 3,3	0.155 ± 0.414	0.004 ± 0.037	1.99E-12	1.129E-07 ± 3.859E-07	4.548E-06 ± 9.942E-06	6.90E-28	-0.4940 ± 1.4705	-0.926± 1.616	7.23E-05
	RCMFE (SD)								
2, 4,3	0.199 ± 0.440	0.013± 0.051	9.55E-12	0.694 ± 5.584E-04	0.696± 0.004	1.67E-30	-0.690± 0.381	-0.892 ± 0.400	4.45E-07

P − value (4.19E-40) with mean ± SD = −0.9163 ± 1.1292E-07 for NSCLC and mean ± SD = -0.9163 ± 4.2841E-06 for SCLC. For EFD features we get significant result at scale 5 having P − value (1.04E-13) with mean ± SD = 2.1503 ± 4.3693 for NSCLC and mean ± SD = 0.0920 ± 0.6323 for SCLC.
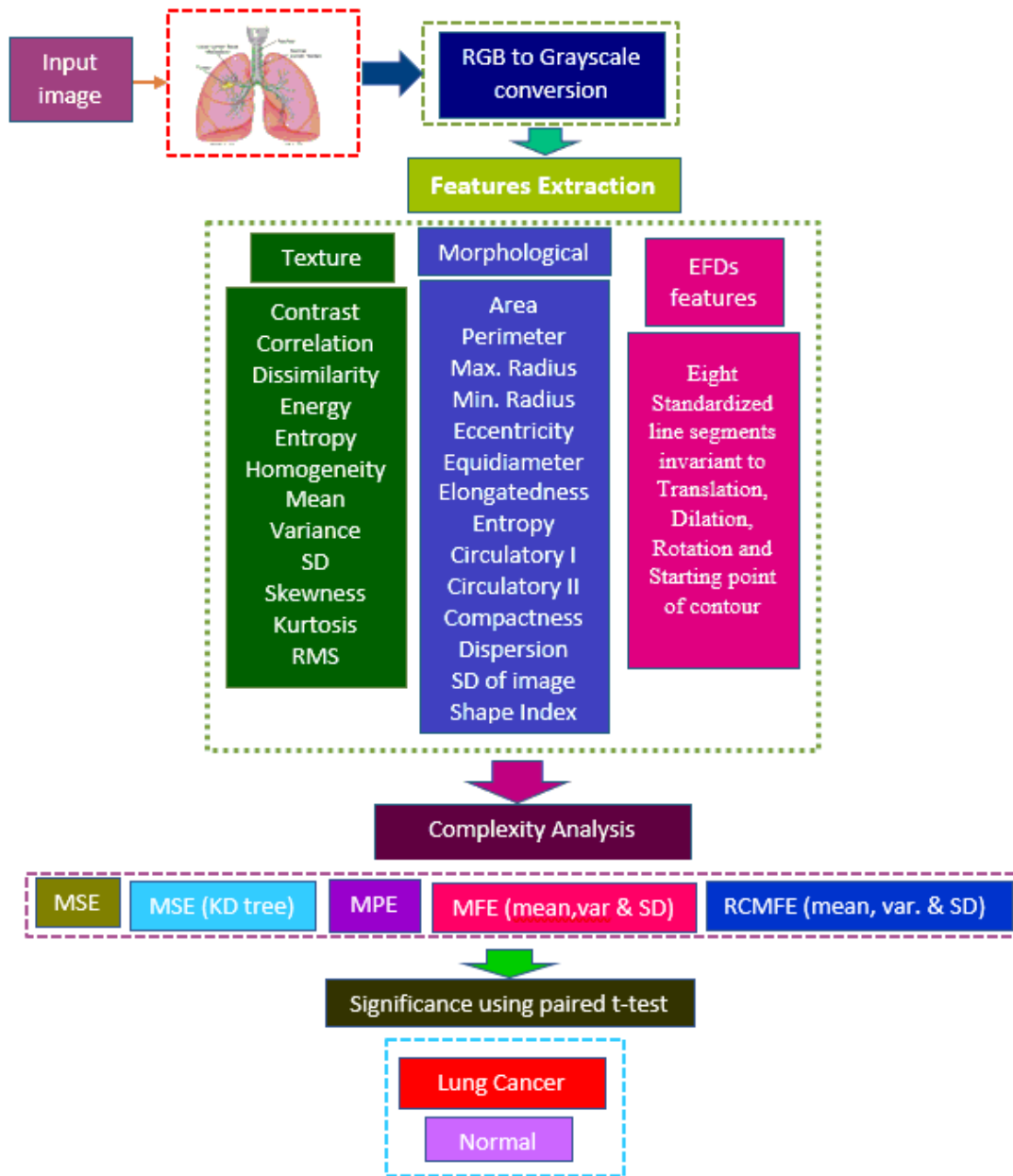
FIGURE 3. Schematic diagram for analyzing the dynamics of lung cancer imaging data by extracting different features and employing entropy-based complexity measures.

As depicted in Table 3, by applying MSE with K-D tree algorithmic approach and extracting morphological features, NSCLC (0.275) exhibit higher entropy than SCLC (0.218). However, in case of texture and EFDs features, SCLC (0.434, 0.853) exhibit higher entropy values than NSCLC (0.102, 0.641) respectively.

The Table 3, we first extracted different features such as texture, morphological and EFDs from lung cancer images and then applied complexity-based measures such as MSE, MPE, MSE with KD tree algorithmic approach, MFE (with mean, variance & SD) and RCMFE (with mean, variance and SD) at multiple temporal scales to distinguish NSCLC

from SCLC images. The highest significant results using MSE by extracting morphological features was obtained at scale 2 with P-value (5.21E-11), texture features with p-value (5.48E-07), and EFDs features with P-value (4.08E-07). By employing MPE the highest significant separation was obtained by extracting morphological features was obtained at scale 2 with P-value (2.50E-03), texture features at scale 1 with P-value (7.58E-04), and EFDs features at scale 1 with P-value (3.78E-12). Likewise, using MSE with KD tree algorithmic approach, the highest significant results were obtained by extracting morphological features at scale 1 with P-value (4.43E-11), texture features at scale 2 with
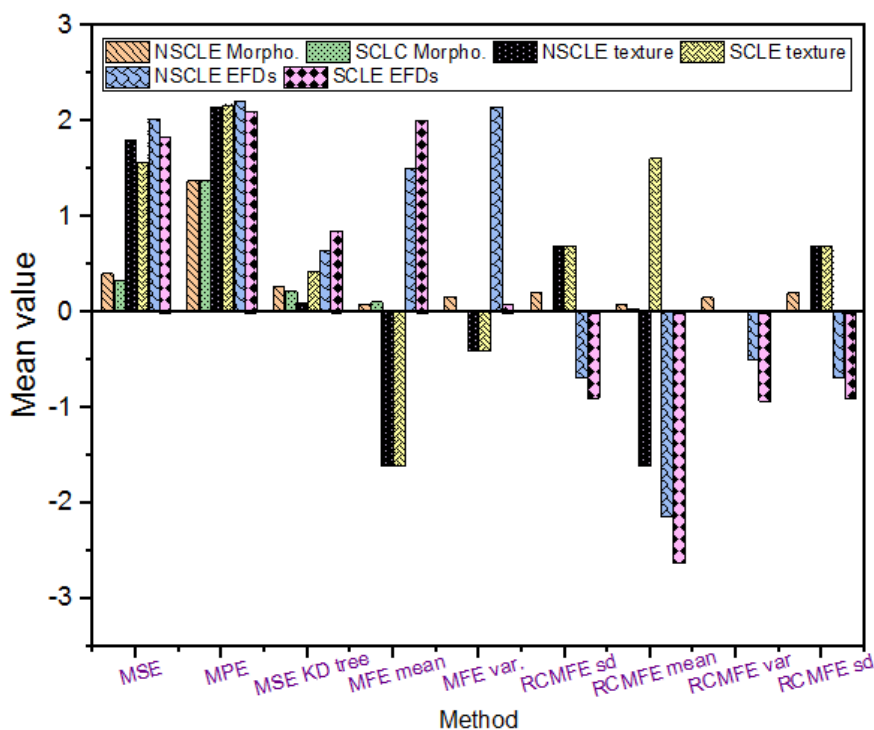
FIGURE 4. Mean values for NSCLC and SCLC subjects by extracting morphological, texture and EFDs features and employing different complexity measures.

P-value (6.21E-16) and EFDs features at scale 7 with P-value (2.06E-06). By employing the MFE with mean, the highest significant results were obtained by extracting morphological features at scale 1 with P-value (3.01E-14), texture features at scale 1 with P-value (9.81E-34) and EFDs features at scale 5 with P-value (2.46E-09). Likewise, by employing MFE with variance, the highest detection results were obtained by extracting morphological features at scale 2 with P-value (2.55E-12), texture features at scale 3 with P-value (3.25E-36), and EFDs features at scale 5 with P-value (1.04E-13). Moreover, by employing MFE with standard deviation, the highest detection performance was obtained by extracting morphological features at scale 2 with P-value (1.16E-10), texture features at scale 2 with P-value (1.95E-50), and EFDs features at scale 2 with P-value (1.82E-12). To distinguish the NSCLC from SCLC, we employed RCMFE with mean, variance and standard deviation. By employing RCMFE with mean, the highest significant results were obtained at scale 1 using morphological features with P-value (3.01E-14), texture features at scale 1 with P-value (9.81E-34) and EFDs features with P-value (3.89E-05). Likewise, detection performance on the basis of significant results by employing RCMFE with variance was obtained at scale 2 by extracting morphological features with P-value (1.99E-12), texture features at scale 3 with P-value (6.90E-28), EFDs features at scale3 with P-value (7.23E-05). Similarly, the highest performance using RCMFE with standard deviation was obtained using morphological features at

scale 2 with P-value (9.55E-12), texture features at scale 4 with P-value (1.67E-30) and EFDs features at scale 3 with P-value (4.45E-07).

The most commonly used types of NSCLC [86] are stated below:

Adenocarcinomas is a common kind of lung cancer seen in Cigarette smoker and in non-smokers. It rises to take place in the edge of the lungs which is due to the addition of filters in cigarettes preventing large particles from entering the lungs. Adenocarcinoma have the capacity to grow slower and a greater chance to be detect before it is spread.

Squamous cell carcinomas more frequent as compared to adenocarcinomas. Squamous cell tumors rise utmost often in the middle chest area. This kind of lung cancer extremely stays inside the lung. These cell carcinomas are also linked to smoking.

Large cell carcinomas, occasionally mentioned as undistinguishable cancer, are the smallest common kind of NSCLC. This type of cancer has a higher chance to be spread on distant places but slowly. The NSCLC and SCLC visual information is shown in the Figure 2 below:

The Figure 3 illustrate the schematic flow of our model. In the first step, we converted the RGB images to grey color. We extracted texture, morphological and EFDs features from NSCLC and SCLC images. The texture features comprised of contrast, correlation, dissimilarity, energy, entropy, homogeneity, mean, variance, standard deviation, kurtosis, and root mean square (RMS). Moreover, the morphological features

comprised of area, perimeter, maximum radius, minimum radius, eccentricity, Equidiameter, Elongatedness, entropy, circulatory I, circulatory II, dispersion, standard deviation of image and shape index and EFDs features which are rely on chain code by approximating shape of closed contour by a sequence of eight standardized line segments and are invariant to translation, dilation, rotation and starting point of contour. We then applied the complexity measures such as multiscale sample entropy (MSE) with mean and KD tree algorithm approach, multiscale permutation entropy (MPE), multiscale fuzzy entropy (MFE) and Refined composite multiscale fuzzy entropy (RCMFE) with mean variance and standard deviation.

The mean values at selected scales were computed as reflected in Table 3 and Figure 4. Mostly, the mean entropy values of NSCLC are greater than SCLC, which shows that NSCLC is complex than SCLC extracted using morphological, texture and EFDs features. By employing MSE, the mean value by extracting morphological features, was obtained as NSCLC (0.405), SCLC (0.3397); texture feature as NSCLC (1.7964), SCLC (1.572); EFDs features as NSCLC (2.0266), SCLC (1.846). Likewise, by employing MPE, the mean value by extracting morphological features was obtained as NSCLC (1.373), SCLC (1.386); texture features as NSCLC (2.151), SCLC (2.18); EFDs features as NSCLC (2.218), SCLC (2.112). By employing MSE with KD tree algorithm, the mean value by extracting morphological feature was obtained as NSCLE (0.275), SCLC (0.218), MFE variance as NSCLC (0.164), SCLC (0.003); MFE standard deviation as NSCLC (0.238), SCLC (0.014); RCMFE with mean as NSCLC (0.082), SCLC (0.0297); RCMFE with variance as NSCLC (0.155), SCLC (0.004); RCMFE with standard deviation as NSCLC (0.199), SCLC (0.013). The values for other complexity measures are reflected in the Table 3 and Figure 4.

IV. DISCUSSION AND CONCLUSION

In the past, researchers applied different complexity measures to quantify the dynamics of highly complex and non-linear dynamical measures by applying Multiscale sample entropy (MSE), MPE, symbolic entropy and refined Fuzzy entropy measures, time-frequency representation measures for detecting epileptic seizures, arrhythmia, heart rate failure, gait dynamics etc. [39], [40], [45]–[48], [56], [87]. The entropy-based complexity measures have been used in diverse fields to quantify the dynamics of highly nonlinear physiological and neurophysiological signals and systems. Single entropy-based measures have some limitations which are alleviated by Costa and Goldberger by introducing new approach as Multiscale sample entropy (MSE) at multiple temporal scales. Moreover, recently, researchers [84] introduced variants of MSE based on variance MSEσ2. Moreover, Hussain recently employed [39] MSE with KD tree algorithmic approach which is more efficient than traditional MSE due to its robustness in time and space complexity and outperformance. Moreover, in short biological signals, the use of MSE produce undefined and inaccurate results [69], [88].

This problem was addressed by employing refined composite MSEμ (RCMSEμ) using the average sample entropy values of several coarse-grained signals in each scale factor [69]. The RCMSEμ produced better results than MSEμ, however their exist a problem of undefined values for short signals [69].

This problem was addressed by proposing a composite multiscale fuzzy entropy (RCMFE) based on μ and σ with an aim to provide more accurate and stable results than the traditional entropy measures. RCMFEμ and RCMFEσ were applied to distinguish the AD from control subjects and provides accuracy of 72.81% and 78.22% respectively. Most recently, Hussain extracted Hybrid features using Refined Fuzzy entropy to detect the arrhythmia. The results revealed that Refined Fuzzy outer performed than traditional entropy measures. A highest detection accuracy with sensitivity (100%), specificity (100%) and accuracy (100%) was obtained by extracting refined fuzzy and composite multiscale entropies with mean, variance and standard deviation.

Lung carcinoma is one of the most lethal of cancers worldwide [89]. Positron emission tomography (PET) data has greater sensitivity and specificity in the staging of lung cancer than computed tomography (CT) or magnetic resonance imaging (MRI). By using k- nearest neighbor and support vector machines (SVM) classifiers. Wavelet features with SVM classifier gave a consistent accuracy of 97% with an average sensitivity and specificity of 81% and 99% respectively. Automatic lung nodule detection scheme in [90] is presented in Multi-Slice Computed Tomography (MSCT) scans using SVM. An automatic CAD system is developed for early detection of lung nodule by analyzing lung CT images which achieves 80% result accuracy [91].

Based on the feature extraction approach, researchers employed machine learning techniques to improve the detection performance. This study is aimed to quantify the complex dynamics of lung cancer types by extracting different features based on structure, spatial arrangement and elliptic shapes. Similarly, in quantifying the dynamics of physiological systems including heart rate variability, electroencephalographic (EEG) signals etc., researchers extracted features based on entropy, fuzzy entropy and other nonlinear measures. Researchers [92] extracted Fuzzy entropy as feature in detecting Coronary Artery Disease (CAD) which are originally proposed by [93] to quantify the dynamics of Heart rate variability signals. It is used in many applications such as epilepsy detection [94], characterizing electromyogram [93] and to distinguish focal and non-focal EEG signals [95]. In past few decades, the nonlinear dynamics of physiological signals were computed using various complexity-based measures from information theoretic approaches. Single entropy measures have limitations for shorter data length. To cope up with this problem, Costa et al. proposed multiscale sample entropy [74], [82], [83]. Recently, researchers employed different complexity-based measures to quantify the dynamics of physiological systems [39], [45], [48], [96]–[98], time-frequency representation methods [46]. Based on the diverse nature of physiological signals, [47] most recently

proposed multimodal features extracting strategy based on time domain, frequency domain, statistical, entropy based using KD-tree algorithmic approach and wavelet based features to detect the epileptic seizure with improved detection performance i.e. accuracy (99.50%), specificity (100%), sensitivity (99%), and area under the receiver operating curve i.e. AUC (0.9950) using K-nearest Neighboring approach which outperformed than the studies of [99] using similar approach, however varying feature selection methods. MSE requires computational complexity of order O (N^2), to cope up this problem, [77] developed MSE with K-d tree algorithmic approach, which is used by [39] and in this study as well require O (N) computational time instead of MSE. Moreover, we have extracted refined Multiscale Fuzzy entropy and refined Multiscale sample entropy features with mean, standard deviation and variance namely (MSE mu, MSE std, MSE var., MFE mu, MFE std, MFE var., RCMSE mu, RCMSE std, RCMSE var.) by taking advantage over recently developed by [68], [100] instead of traditional Fuzzy Entropy features as employed by [92].

The MSE with KD tree algorithmic approach outperformed to distinguished NSCLC from SCLC based on extracted morphological features i.e. MSE with KD tree give P-value (4.43E-11) & MSE with mean give P-value (5.21E-11). Moreover, from extracted texture features, MSE with KD tree provides P-value (6.21E-16) & MSE give P-value (5.48E-7). Similarly, MFE with mean, variance and SD outperformed than traditional MSE with mean and KD algorithmic approaches with extracted morphological and texture features i.e. MFE with mean give significant results of P-value (3.01E-14, 9.81E-34) from extracted morphological and texture features respectively.

By extracting texture features from Lung cancer images, the order of separation was obtained in the following order, the MFE with SD p-value (1.95E-50) followed by MSE with variance P-value (3.25E-36), MFE & RCMFE with mean P-value (9.81E-34), RCMFE with SD P-value (1.67E-30), RCMFE with variance P-value (6.90E-28) at the selected scales where optimal results were obtained. Moreover, by extracting morphological features the highest detection separation was obtained using MFE & RCMFE with mean P-value (3.01E-14) followed by RCMFE with variance P-value (1.99E-12), MFE with variance P-value 2.55E-12), MSE with KD tree P-value (4.43E-11), MSE with mean P-value (5.21E-11), MFE with SD provide P-value (1.16E-10). Likewise by extracting EFDs features, the highest separation was obtained using MFE with variance P-value (1.04E-13), followed by MFE with SD P-value (1.82E-12), MPE P-value (3.78E-12), MFE with mean P-value (2.46E-09), MSE with mean P-value (4.08E-7), MSE with KD tree P-value (2.06E-60 and RCMFE P-value (3.89E-5).

The physiological system is comprised of different subsystems being controlled by the regularity mechanism of that system [83], [101]–[103]. If all the subsystems are properly functional and working, the control mechanism of that system will be appropriate and system is healthy. The healthy system

evolve with time and their adaptive capability is higher which result in higher complexity. The alternative is the structural components and / or decreased functional capability of the subsystem resulting in dysfunction of the regularity mechanism of the overall systems thereby decrease in complexity. For example, in the human inner ear, the loss of high frequency sound may be caused by alteration in sound receptors, blood supply, neurons, or in the structural changes of the basilar membrane in the inner ear [104].

To determine the complexity of a system, a number of independent variables are required to predict or produce the output of the system. For example, in the skeletal muscle the fiber type expression is dependent on the hormonal, genetic, neuronal, cardiovascular and activity related influences that affect the fast or slow myosin isoform expression in the muscle [105], [106]. The structural components loss is analogous to losing a component variable. To understand the structural component loss, consider an example of dynamics changes due to the loss of dopaminergic cells in the substantia nigra compacta of the Basel ganglia occurring with age and Parkinson's disease. About 80% if the dopaminergic cells in the Parkinson's disease die before most of the behavioral symptoms of Parkinson's disease are observed [107]. This reduce the outflow from internal globus pallidus of the Basel ganglia due to reduction in the dopamine cells and is related to the loss of complexity observed in the tremor output of individuals with Parkinson's disease [108], [109].

There are several examples of reduction of structural components with aging disease including collagen fibers per unit of surface area in skin tissue [110], estrogen hormone activity in females [111], sinus node cells in the heart [112], the number of alveoli of the lungs [113], [114], physical brain damage or even death may happen due to the frequently occurrence of seizures [44], [45], chronic alcohol drinking cause alcohol-related brain damage (ARBD) including brain structure change [39]. The coupling functions between the structural components can influence the dynamics in a system due to the synchronization between the motor units [115], [116]. The motor unit include muscle fibers, nerve and neuromuscular junction where muscle and never fibers communication [117], [118]. The motor unit synchrony changes would represent the altered coupling between the structural components of the nervous systems.

In this study, we extracted the morphological, texture and EFDs features by considering different aspects such as structure and geometry of cancerous images, spatial arrangement of cancer images intensities and ellipse-based characteristics. The researchers in the past extracted different features extracting strategies and classify different machine learning classification measures based on features extracting approaches. However, we aim in this study to quantify the further dynamics of different features extracting strategies by computing the nonlinear dynamics present in the cancer imaging datasets. We applied multiscale sample entropy (MSE) with mean and K-D tree algorithmic approach, Multiscale permutation entropy (MPE), multiscale

TABLE 4. Morphological features.

Morphological Features	Mathematical Equations	Descriptions
Area (A)	Total amount of Pixel of image	The total Number of pixels in the image
Perimeter (P)	The amount of Pixel at the boundary of the image	The total amount of pixel at the boundary of an image which differentiate the regular image from irregular image
Maximum Radius (MAX_R)	The maximum distance between center and boundary of an image. MAX(DISTANCE(C(x,y), BOUNDARY(x,y)))	To calculate maximum distance between center of an image to the boundary of an image
Minimum Radius (MIN_R)	The minimum distance between center and boundary of an image. MIN(DISTANCE(C(x,y), BOUNDARY(x,y)))	To calculate minimum distance between center of an image to the boundary of an image. where x and y are points on the image
Euler Number (EUL_NO)	No of effected region of an image – No of uneffected region of an image	It is the difference between the effected region of an image and unaffected region of an image
Eccentricity (ECT)	$\sqrt{1-\left(\frac{MIN\_R}{MAX\_R}\right)^2}$	It is used for the lengthening of an image
Equivdiameter (EQD)	$\sqrt{4*\frac{Area}{\pi}}$	It is used to calculate diameter of a circle which has same area as an image
Elongatedness (EN)	$\left(\frac{Area}{(2*MAX\_R)^2}\right)$	Elogatendness of an image is ratio of length of an image to its thickness square.
Entropy (ENTPY)	$\sum\left(p*log_2(p)\right)^2$	It is a statistical measure of randomness which is used to characterize the texture of the image.
Circularity1 (C_1)	$\sqrt{\frac{Area}{\pi*MAX\_R^2}}$	It is used to show how an image is resemble as circle
Circularity1 (C_2)	$\sqrt{\frac{MIN\_R}{MAX\_R}}$	It is used to show how an image is resemble as ellipse
Compactness (CN)	$\left(\frac{2*\sqrt{Area*\pi}}{Perimeter}\right)$	It is used to calculate the degree of deviation of an image from a Perfect Circle
Dispersion (DP)	$\left(\frac{MAX\_R}{Area}\right)$	It is used to measure the irregularity of an image
Standard Deviation of Image (SD)	$\sqrt{\frac{1}{n}\sum_{i=1}^{n}(x_i-\bar{x})^2}$	It is used to measure the average contrast of an image
Shape Index (SI)	$\left(\frac{Perimeter}{2*MAX\_R}\right)$	It is relates to curved states of an image

fuzzy entropy (MFE) and refined composite multiscale fuzzy entropy (RCMFE) based on mean, standard deviation and variance to quantify the dynamics at multiple temporal scales.

As these nonlinear dynamical measures have been successfully used in many applications to quantify the dynamics of heart rate variability, arrhythmia, epilepsy, gait dynamics,

TABLE 5. Texture features.

S#	Texture Features	Formulas	Description
1	Contrast	$\sum_{x,y=0}^{N-1} P_{x,y}\,(x-y)^2$	It is used to calculate the intensity contrast b/w a pixel and its neighbor one of the whole images
2	Correlation	$\sum_{x,y=0}^{N-1} P_{x,y} \left[\dfrac{(x-\mu_x)(y-\mu_y)}{\sqrt{(\sigma_x^2)(\sigma_y^2)}} \right]$	It is used to calculate the degree of correlation b/w pixel and its neighbor one of the whole images
3	Dissimilarity	$\sum_{x,y=0}^{N-1} P_{x,y}\,|x-y|$	To calculate the difference in images
4	Energy	$\sum_{x,y=0}^{N-1} P_{x,y}^2$	It is used to calculate the uniformity of an image
5	Entropy	$\sum_{x,y=0}^{N-1} P_{x,y}\,(-ln P_{x,y})$	It is used to calculate the information encoded in the image
6	Homogeneity	$\sum_{x,y=0}^{N-1} \dfrac{P_{x,y}}{1+(x-y)^2}$	It is used to calculate the spatial closeness of the distribution of elements in G to the diagonal.
7	Mean	$\mu_x = \sum_{x,y=0}^{N-1} x\,(P_{x,y})$ & $\mu_y = \sum_{x,y=0}^{N-1} y\,(P_{x,y})$	It is used to calculate the sum of all possible images and P is the probability mass function.
8	Variance	$\sigma_x^2 = \sum_{x,y=0}^{N-1} P_{x,y}\,(x-\mu_x)^2$ & $\sigma_y^2 = \sum_{x,y=0}^{N-1} P_{x,y}\,(y-\mu_y)^2$	It is used to calculate how far a set of (random) numbers are spread out from their mean
9	Standard Deviation	$\sigma_x = \sqrt{\sigma_x^2}$ & $\sigma_y = \sqrt{\sigma_y^2}$	It is used to calculate to quantify the amount of variation or dispersion of a set of data values
10	Skewness	$\dfrac{1}{N \times N} \sum_{i=0}^{N} \sum_{j=0}^{N} \left[\dfrac{p(i,j)-\mu}{\sigma} \right]^3$	Skewness is used to obtain the degree of asymmetry of any pixel around its mean.
11	Kurtosis	$\dfrac{1}{N \times N} \sum_{i=0}^{N} \sum_{j=0}^{N} \left[\dfrac{p(i,j)-\mu}{\sigma} \right]^4$	This formula can compute the flatness or peakness of a distribution.
12	RMS	$\sqrt{\dfrac{p(i,j)^2}{N \times N}}$	Root mean square (RMS) is used to calculate the error between known and predicted value.

human activity dynamics, and brain dynamics. The small cell lung cancer (SCLC) spread more faster to the other organs than non small cell lung cancer (NSCLC) type. Patients sometime may not early experience the symptoms associated with lung cancer until cancer reached at its advanced stage. Based on the recent findings, the NSCLC contain more complex dynamics, spread slowly than the SCLC type which spread very rapidly. Based on the findings of the recent study by applying multiscale entropy measures to quantify the dynamics for early diagnosis and prognosis of NSCLC can help the radiologists, oncologists and medical specialists to further promulgation towards advanced stages. The results further reveal that NSCLC based on the robust complexity measures exhibit complex dynamics at multiple temporal scales which can further studied for more comprehensive analysis. The findings also consistent with the previous studies. Recently, Hussain computed the complexity of epileptic subjects (ictal intervals- with seizure) and epileptic subjects (interictal interval – without seizures) and obtained that interictal interval subjects contain more complex dynamics than the ictal interval subjects with seizures. The interictal interval can be focal and non-focal signals effecting only part of body, which may be converted to generalized seizures by effecting whole body. Lung cancer is categorized in two types i.e. NSCLC type which is present in 85 % and SCLC type in 15%, which are classified [43] based on different features extraction approaches as proposed by [18], [20] and employing machine learning techniques. However,

NSCLC having complex dynamics can be transformed to SCLC [2] if not properly and timely treated. This study reveals that complexity measure can help us to further quantify the dynamics of these two cancer types. The findings of the recent study shows that refined fuzzy entropy [68], [100] instead of traditional Fuzzy Entropy features as employed by [92] exhibit higher separation to distinguish the NSCLC and SCLC that traditional entropy measures.

Lung cancer is the most severe cancers in the world with the minimum survival ratio after the analysis [119]. It is the most common cause of life internationally. The incidence of lung cancers has multiplied unexpectedly and come to be the most common cancer in maximum countries. The research is done in order to separate SCLC groups from that of NSCLC groups using the entropy-based method with various features extraction techniques i.e. Texture Feature, Morphological feature, and Elliptic Fourier Descriptors (EFDs. Using these entropy measures, we calculated Mean, Standard deviation and P-value at different scales against each group (NSCLC and SCLC) on the basis of extracted features values. The minimum P-value against the groups shows the most significant results and exhibit the good separation between the groups. The greater mean value shows the higher complexity for the class. If we compare all the results extracted using Texture feature between two groups (NSCLC AND SCLC), then we clearly say that the more significant value is obtained using MFE with SD having minimum P-value (1.95E-50). By extracting morphological features, the highest separation was obtained using MFE with mean having minimum P-value (3.01E-14). The results indicated that entropy measures are a very helpful methods to measure the dynamics of lung cancer for early detection and prognosis.

LIMITATIONS AND FUTURE RECOMMENDATIONS

In the present study, we distinguish the NSCLC from SCLC only based on available lung cancer imaging database by employing various non-linear dynamical measures. In future, we will compare the dynamics of both types of cancers with healthy lung cells.

APPENDIX//ANNEX-A

See table 4 and 5.

REFERENCES

[1] R. L. Siegel, K. D. Miller, and A. Jemal, "Cancer statistics, 2018," *CA, Cancer J. Clin.*, vol. 68, no. 1, pp. 7–30, Jan. 2018.

[2] M. G. Oser, M. J. Niederst, L. V. Sequist, and J. A. Engelman, "Transformation from non-small-cell lung cancer to small-cell lung cancer: Molecular drivers and cells of origin," *Lancet Oncol.*, vol. 16, no. 4, pp. e165–e172, Apr. 2015.

[3] V. Krishnaiah, G. Narsimha, and N. C. Subhash, "Diagnosis of lung cancer prediction system using data mining classification techniques," *Int. J. Comput. Sci. Inf. Technol.*, vol. 4, no. 1, pp. 39–45, 2013.

[4] C. González-Forteza *et al.*, "Confiabilidad y validez de la escala de depresión CES-D en un censo de estudiantes de nivel medio superior y superior, en la Ciudad de MÃ©xico," *Salud Mental*, vol. 34, no. 1, pp. 53–59, 2011.

[5] S. Thummajitsakul, W. Kaewsri, and P. Deetae, "Analysis of intraspecific genetic variation, antioxidant and antibacterial activities of Zingiber zerumbet," *Int. Food Res. J.*, vol. 23, no. 4, pp. 1552–1557, 2016.

[6] G. A. Silvestri *et al.*, "Noninvasive staging of non-small cell lung cancer: ACCP evidenced-based clinical practice guidelines (2nd edition)," *Chest*, vol. 132, no. 3, pp. 178S–201S, 2007.

[7] W. D. Travis *et al.*, "International association for the study of lung cancer/American thoracic society/European respiratory society: International multidisciplinary classification of lung adenocarcinoma: Executive summary," *Amer. Thoracic Soc.*, vol. 8, no. 5, pp. 381–385, 2011.

[8] P. S. Loo, S. C. Thomas, M. C. Nicolson, M. N. Fyfe, and K. M. Kerr, "Subtyping of undifferentiated non-small cell carcinomas in bronchial biopsy specimens," *J. Thoracic Oncol.*, vol. 5, no. 4, pp. 442–447, 2010.

[9] A. G. Nicholson *et al.*, "Refining the diagnosis and EGFR status of non-small cell lung carcinoma in biopsy and cytologic material, using a panel of mucin staining, TTF-1, cytokeratin 5/6, and P63, and EGFR mutation analysis," *J. Thorac. Oncol.*, vol. 5, no. 4, pp. 436–441, 2010.

[10] S. A. El-Regaily, M. A. Salem, M. H. A. Aziz, and M. I. Roushdy, "Survey of computer aided detection systems for lung cancer in computed tomography," *Current Med. Imag. Rev.*, vol. 14, no. 1, pp. 3–18, Nov. 2017.

[11] H. Shao, L. Cao, and Y. Liu, "A detection approach for solitary pulmonary nodules based on CT images," in *Proc. 2nd Int. Conf. Comput. Sci. Netw. Technol.*, Dec. 2012, pp. 1253–1257.

[12] J. A. Cruz and D. S. Wishart, "Applications of machine learning in cancer prediction and prognosis," *Cancer Inform.*, vol. 2, pp. 59–77, Jan. 2006.

[13] B. Muthazhagan and T. Ravi, "An early diagnosis of lung cancer disease using data mining and medical image processing methods: A survey," *Middle-East J. Sci. Res.*, vol. 24, no. 10, pp. 3263–3267, 2016.

[14] Y. Lee, T. Hara, H. Fujita, S. Itoh, and T. Ishigaki, "Automated detection of pulmonary nodules in helical CT images based on an improved template-matching technique," *IEEE Trans. Med. Imag.*, vol. 20, no. 7, pp. 595–604, Jul. 2001.

[15] A. El-Baz *et al.*, "Computer-aided diagnosis systems for lung cancer: Challenges and methodologies," *Int. J. Biomed. Imag.*, vol. 2013, Nov. 2013, Art. no. 942353.

[16] S. O. Friedrich, F. von Groote-Bidlingmaier, and A. H. Diacon, "Xpert MTB/RIF assay for diagnosis of pleural tuberculosis," *J. Clin. Microbiol.*, vol. 49, no. 12, pp. 4341–4342, Dec. 2011.

[17] S. Rathore, M. Hussain, M. A. Iftikhar, and A. Jalil, "Ensemble classification of colon biopsy images based on information rich hybrid features," *Comput. Biol. Med.*, vol. 47, no. 1, pp. 76–92, 2014.

[18] S. Rathore, M. Hussain, and A. Khan, "Automated colon cancer detection using hybrid of novel geometric features and some traditional features," *Comput. Biol. Med.*, vol. 65, pp. 279–296, Oct. 2015.

[19] S. Rathore, A. Iftikhar, A. Ali, M. Hussain, and A. Jalil, "Capture largest included circles: An approach for counting red blood cells," *Emerging Trends and Applications in Information Communication Technologies* (Communications in Computer and Information Science), vol. 281. Berlin, Germany: Springer, 2012, pp. 373–384.

[20] L. Hussain *et al.*, "Prostate cancer detection using machine learning techniques by employing combination of features extracting strategies," *Cancer Biomarkers*, vol. 21, no. 2, pp. 393–413, Feb. 2018.

[21] Y. Asim, B. Raza, A. K. Malik, S. Rathore, L. Hussain, and M. A. Iftikhar, "A multi-modal, multi-atlas-based approach for Alzheimer detection via machine learning," *Int. J. Imag. Syst. Technol.*, vol. 28, no. 2, pp. 113–123, 2018.

[22] P. N. Kugler and M. T. Turvey, *Information, Natural Law, and the Self-Assembly of Rhythmic Movement*. Abingdon, U.K.: Routledge, 2015.

[23] J. Wallman, "A minimal visual restriction experiment: Preventing chicks from seeing their feet affects later responses to mealworms," *Develop. Psychobiol.*, vol. 12, no. 4, pp. 391–397, Jul. 1979.

[24] M. Guevara, L. Glass, and A. Shrier, "Phase locking, period-doubling bifurcations, and irregular dynamics in periodically stimulated cardiac cells," *Science*, vol. 214, no. 4527, pp. 1350–1353, Dec. 1981.

[25] J. A. S. Kelso, A. J. Mandell, and M. F. Shlesinger, *Dynamic Patterns In Complex Systems*. Fort Lauderdale, FL, USA: World Scientific, 1988, pp. 1–432.

[26] F. E. Yates, "The dynamics of adaptation in living systems," in *Adaptive Control of Ill-Defined Systems*. Boston, MA, USA: Springer, 1984, pp. 89–113.

[27] A. L. Goldberger and B. J. West, "Fractals in physiology and medicine," *Yale J. Biol. Med.*, vol. 60, no. 5, pp. 421–435, 1987.

[28] R. A. Heath, *Nonlinear Dynamics*. London, U.K.: Psychology Press, 2014.

[29] D. Kaplan, L. Glass, and S. A. Berger, "Understanding nonlinear dynamics," *Phys. Today*, vol. 49, no. 2, p. 62, Feb. 1996.

[30] S. M. Pincus, "Approximate entropy as a measure of system complexity," *Proc. Natl. Acad. Sci.*, vol. 88, no. 6, pp. 2297–2301, Mar. 1991.

[31] P. Grassberger and I. Procaccia, "Measuring the strangeness of strange attractors," *Phys. D, Nonlinear Phenomena*, vol. 9, no. 1, pp. 189–208, Oct. 1983.

[32] E. B. Hall, A. E. Wessel, and G. L. Wise, "Some aspects of fusion in estimation theory," *IEEE Trans. Inf. Theory*, vol. 37, no. 2, pp. 420–422, Mar. 1991.

[33] F. Takens, "Detecting strange attractors in turbulence," *Dynamical Systems and Turbulence, Warwick*, vol. 981. Berlin, Germany: Springer, 1980, pp. 366–381.

[34] D. S. Bassett, N. F. Wymbs, M. P. Rombach, M. A. Porter, P. J. Mucha, and S. T. Grafton, "Task-based core-periphery organization of human brain dynamics," *PLoS Comput. Biol.*, vol. 9, no. 9, Sep. 2013, Art. no. e1003171.

[35] L. A. Lipsitz, "Loss of 'complexity' and aging potential applications of fractals and chaos theory to senescence," *JAMA*, vol. 267, no. 13, p. 1806, Apr. 1992.

[36] Y. Hayashi, "Space-time spectral analysis and its applications to atmospheric waves," *J. Meteorol. Soc. Jpn., II*, vol. 60, no. 1, pp. 156–171, 1982.

[37] K. Briggs, "An improved method for estimating Liapunov exponents of chaotic time series," *Phys. Rev. A, Gen. Phys.*, vol. 151, nos. 1–2, pp. 27–32, Nov. 1990.

[38] J. M. Hausdorff, C. K. Peng, Z. Ladin, J. Y. Wei, and A. L. Goldberger, "Is walking a random walk? Evidence for long-range correlations in stride interval of human gait," *J. Appl. Physiol.*, vol. 78, no. 1, pp. 349–358, Jan. 1995.

[39] L. Hussain *et al.*, "Quantifying the dynamics of electroencephalographic (EEG) signals to distinguish alcoholic and non-alcoholic subjects using an MSE based K-d tree algorithm," *Biomed. Eng./Biomedizinische Technik*, vol. 63, no. 4, pp. 481–490, Jul. 2018.

[40] L. Hussain, W. Aziz, S. Saeed, I. A. Awan, A. A. Abbasi, and N. Maroof, "Arrhythmia detection by extracting hybrid features based on refined Fuzzy entropy (FuzEn) approach and employing machine learning techniques," *Waves Random Complex Media*, pp. 1–31, Dec. 2018.

[41] L. Hussain, W. Aziz, S. Saeed, S. Rathore, and M. Rafique, "Automated breast cancer detection using machine learning techniques by extracting different feature extracting strategies," in *Proc. 17th IEEE Int. Conf. Trust, Secur. Privacy Comput. Commun./12th IEEE Int. Conf. Big Data Sci. Eng. (TrustCom/BigDataSE)*, Aug. 2018, pp. 327–331.

[42] L. Hussain, S. Saeed, I. A. Awan, A. Idris, M. S. A. Nadeem, and Q.-A. Chaudhry, "Detecting brain tumor using machine learning techniques based on different features extracting strategies," *Current Med. Imag. Rev.*, vol. 14, no. 1, pp. 1–14, 2018.

[43] L. Hussain, S. Rathore, A. A. Abbasi, and S. Saeed, "Automated lung cancer detection based on multimodal features extracting strategy using machine learning techniques," *Proc. SPIE*, vol. 10948, Mar. 2019, Art. no. 109483Q.

[44] L. Hussain, S. Saeed, I. A. Awan, and A. Idris, "Multiscaled complexity analysis of EEG epileptic seizure using entropy-based techniques," *Arch. Neurosci.*, vol. 5, no. 1, pp. 1–11, Jan. 2018.

[45] L. Hussain *et al.*, "Symbolic time series analysis of electroencephalographic (EEG) epileptic seizure and brain dynamics with eye-open and eye-closed subjects during resting states," *J. Physiol. Anthropol.*, vol. 36, no. 1, p. 21, Mar. 2017.

[46] L. Hussain *et al.*, "Spatial wavelet-based coherence and coupling in EEG signals with eye open and closed during resting state," *IEEE Access*, vol. 6, no. 3, pp. 37003–37022, 2018.

[47] L. Hussain, "Detecting epileptic seizure with different feature extracting strategies using robust machine learning classification techniques by applying advance parameter optimization approach," *Cogn. Neurodyn.*, vol. 12, no. 3, pp. 271–294, Jun. 2018.

[48] L. Hussain *et al.*, "Complexity analysis of EEG motor movement with eye open and close subjects using multiscale permutation entropy (MPE) technique," *Biomed. Res.*, vol. 28, no. 16, pp. 7104–7111, 2017.

[49] L. Hussain *et al.*, "Regression analysis for detecting epileptic seizure with different feature extracting strategies," *Biomed. Eng. Tech.*, pp. 1–23, May 2019.

[50] F. Khalvati, J. Zhang, A. G. Chung, M. J. Shafiee, A. Wong, and M. A. Haider, "MPCaD: A multi-scale radiomics-driven framework for automated prostate cancer localization and detection," *BMC Med. Imag.*, vol. 18, no. 1, p. 16, May 2018.

[51] V. Fetz, H. Prochnow, M. Brönstrup, and F. Sasse, "Target identification by image analysis," *Nat. Product Rep.*, vol. 33, no. 5, pp. 655–667, 2016.

[52] M. M. Usaj, E. B. Styles, A. J. Verster, H. Friesen, C. Boone, and B. J. Andrews, "High-content screening for quantitative cell biology," *Trends Cell Biol.*, vol. 26, no. 8, pp. 598–611, Aug. 2016.

[53] M. Boutros, F. Heigwer, and C. Laufer, "Microscopy-based high-content screening," *Cell*, vol. 163, no. 6, pp. 1314–1325, Dec. 2015.

[54] T. Kadir and F. Gleeson, "Lung cancer prediction using machine learning and advanced imaging techniques," *Transl. Lung Cancer Res.*, vol. 7, no. 3, p. 304, 2018.

[55] D. G. Fatouros *et al.*, "Structural development of self nano emulsifying drug delivery systems (SNEDDS) during *in vitro* lipid digestion monitored by small-angle X-ray scattering," *Pharmaceutical Res.*, vol. 24, no. 10, pp. 1844–1853, Oct. 2007.

[56] L. Hussain *et al.*, "Applying Bayesian network approach to determine the association between morphological features extracted from prostate cancer images," *IEEE Access*, vol. 7, pp. 1586–1601, 2018.

[57] X. Wang, S. Zhang, and J. Men, "A target recognition method using orthogonal maximum margin criterion projection," *UPB Sci. Bull., D, Mech. Eng.*, vol. 79, pp. 15–26, Jan. 2017.

[58] D. S. Guru, Y. H. Sharath, and S. Manjunath, "Texture features and KNN in classification of flower images," *Int. J. Comput. Appl.*, no. 1, pp. 21–29, Aug. 2010.

[59] S. G. Mougiakakou, I. Valavanis, K. S. Nikita, A. Nikita, and D. Kelekis, "Characterization of CT liver lesions based on texture features and a multiple neural network classification scheme," in *Proc. 25th Annu. Int. Conf. IEEE Eng. Med. Biol. Soc.*, Sep. 2003, pp. 1287–1290.

[60] M. E. Mavroforakis, H. V. Georgiou, D. Cavouras, N. Dimitropoulos, and S. Theodoridis, "Mammographic mass classification using textural features and descriptive diagnostic data," in *Proc. Int. Conf. Digit. Signal Process. (DSP)*, vol. 1, Jul. 2002, pp. 461–464.

[61] A. N. Esgiar, R. N. Naguib, B. S. Sharif, M. K. Bennett, and A. Murray, "Microscopic image analysis for quantitative measurement and feature identification of normal and cancerous colonic mucosa," *IEEE Trans. Inf. Technol. Biomed.*, vol. 2, no. 3, pp. 197–203, Sep. 1998.

[62] A. N. Esgiar, R. N. G. Naguib, B. S. Sharif, M. K. Bennett, and A. Murray, "Fractal analysis in the detection of colonic cancer images," *IEEE Trans. Inf. Technol. Biomed.*, vol. 6, no. 1, pp. 54–58, Mar. 2002.

[63] D. G. Lowe, "Distinctive image features from scale-invariant keypoints," *Int. J. Comput. Vis.*, vol. 60, no. 2, pp. 91–110, Nov. 2004.

[64] F. P. Kuhl and C. R. Giardina, "Elliptic Fourier features of a closed contour," *Comput. Graph. Image Process.*, vol. 18, no. 3, pp. 236–258, Mar. 1982.

[65] L. P. Nicoli and G. C. Anagnostopoulos, "Shape-based recognition of targets in synthetic aperture radar images using elliptical Fourier descriptors," *Proc. SPIE*, vol. 6967, Apr. 2008, Art. no. 69670G.

[66] T. Taxt and K. W. Bjerde, "Classification of handwritten vector symbols using elliptic Fourier descriptors," in *Proc. IEEE 12th IAPR Int. Conf. Pattern Recognit. (Cat. No.94CH3440-5)*, Jerusalem, Israel, vol. 2, Oct. 1994, pp. 123–128.

[67] Y. Yoshioka, H. Iwata, R. Ohsawa, and S. Ninomiya, "Analysis of petal shape variation of primula sieboldii by elliptic Fourier descriptors and principal component analysis," *Ann. Botany*, vol. 94, no. 5, pp. 657–664, Nov. 2004.

[68] H. Azami, A. Fernández, and J. Escudero, "Refined multiscale fuzzy entropy based on standard deviation for biomedical signal analysis," *Med. Biol. Eng., Comput.*, vol. 55, no. 11, pp. 2037–2052, Nov. 2017.

[69] S.-D. Wu, C.-W. Wu, S.-G. Lin, K.-Y. Lee, and C.-K. Peng, "Analysis of complex time series using refined composite multiscale entropy," *Phys. Lett. A*, vol. 378, no. 20, pp. 1369–1374, Apr. 2014.

[70] A. Ben-Mizrachi, I. Procaccia, and P. Grassberger, "Characterization of experimental (noisy) strange attractors," *Phys. Rev. A, Gen. Phys.*, vol. 29, no. 2, pp. 975–977, Feb. 1984.

[71] P. Grassberger, "Finite sample corrections to entropy and dimension estimates," *Phys. Lett. A*, vol. 128, nos. 6–7, pp. 369–373, Apr. 1988.

[72] P. Grassberger and I. Procaccia, "Estimation of the kolmogorov entropy from a chaotic signal," *Phys. Rev. A, Gen. Phys.*, vol. 28, no. 4, pp. 2591–2593, Oct. 1983.

[73] P. Grassberger, T. Schreiber, and C. Schaffrath, "Nonlinear time sequence analysis," *Int. J. Bifurcation Chaos*, vol. 1, no. 3, pp. 521–547, Sep. 1991.

[74] M. Costa, A. L. Goldberger, and C.-K. Peng, "Multiscale entropy analysis of complex physiologic time series.," *Phys. Rev. Lett.*, vol. 89, no. 6, 2002, Art. no. 068102.

[75] G. Manis, "Fast computation of approximate entropy," *Comput. Methods Programs Biomed.*, vol. 91, no. 1, pp. 48–54, Jul. 2008.

[76] C. Silpa-Anan and R. Hartley, "Optimised KD-trees for fast image descriptor matching," in *Proc. IEEE Conf. Comput. Vis. Pattern Recognit.*, Jun. 2008, pp. 1–8.

[77] Y.-H. Pan, W.-Y. Lin, Y.-H. Wang, and K.-T. Lee, "Computing multiscale entropy with orthogonal range search," *J. Mar. Sci. Technol.*, vol. 19, no. 1, pp. 107–113, 2011.

[78] M. Zanin, L. Zunino, O. A. Rosso, and D. Papo, "Permutation entropy and its main biomedical and econophysics applications: A review," *Entropy*, vol. 14, no. 8, pp. 1553–1577, Aug. 2012.

[79] C. Bandt and B. Pompe, "Permutation entropy: A natural complexity measure for time series," *Phys. Rev. Lett.*, vol. 88, no. 17, Apr. 2002, Art. no. 174102.

[80] G. Ouyang, J. Li, X. Liu, and X. Li, "Dynamic characteristics of absence EEG recordings with multiscale permutation entropy analysis," *Epilepsy Res.*, vol. 104, no. 4, pp. 246–252, May 2013.

[81] M. D. Costa, C.-K. Peng, and A. L. Goldberger, "Multiscale analysis of heart rate dynamics: Entropy and time irreversibility measures," *Cardiovascular Eng.*, vol. 8, no. 2, pp. 88–93, 2008.

[82] M. Costa, C. K. Peng, A. L. Goldberger, and J. M. Hausdorff, "Multiscale entropy analysis of human gait dynamics," *Phys. A, Stat. Mech. Appl.*, vol. 330, nos. 1–2, pp. 53–60, 2003.

[83] M. Costa, A. L. Goldberger, and C.-K. Peng, "Multiscale entropy analysis of biological signals," *Phys. Rev. E, Stat. Phys. Plasmas Fluids Relat. Interdiscip. Top.*, vol. 71, no. 2, 2005, Art. no. 021906.

[84] M. D. Costa and A. L. Goldberger, "Generalized multiscale entropy analysis: Application to quantifying the complex volatility of human heartbeat time series," *Entropy*, vol. 17, no. 3, pp. 1197–1203, 2015.

[85] L. Costa and L. Bauer, "Quantitative electroencephalographic differences associated with alcohol, cocaine, heroin and dual-substance dependence," *Drug Alcohol Dependence*, vol. 46, nos. 1–2, pp. 87–93, Jun. 1997.

[86] C. Zappa and S. A. Mousa, "Non-small cell lung cancer: Current treatment and future advances," *Transl. Lung Cancer Res.*, vol. 5, no. 3, pp. 288–300, Jun. 2016.

[87] L. Hussain, W. Aziz, S. A. Nadeem, and A. Q. Abbasi, "Classification of normal and pathological heart signal variability using machine learning techniques classification of normal and pathological heart signal variability using machine learning techniques," *Int. J. Darshan Inst. Eng. Res. Emerg. Technol.*, vol. 3, no. 2, pp. 13–18, Dec. 2014.

[88] L. Angelini *et al.*, "Multiscale analysis of short term heart beat interval, arterial blood pressure, and instantaneous lung volume time series," *Artif. Intell. Med.*, vol. 41, no. 3, pp. 237–250, Nov. 2007.

[89] A. Kanakatte, N. Mani, B. Srinivasan, and J. Gubbi, "Pulmonary tumor volume detection from positron emission tomography images," in *Proc. Int. Conf. BioMed. Eng. Inform.*, 2008, pp. 213–217.

[90] Y. Liu, J. Yang, D. Zhao, and J. Liu, "A method of pulmonary nodule detection utilizing multiple support vector machines," in *Proc. Int. Conf. Comput. Appl. Syst. Model. (ICCASM)*, vol. 10, Oct. 2010, pp. V10-118–V10-121.

[91] S. S. Parveen and C. Kavitha, "Detection of lung cancer nodules using automatic region growing method," in *Proc. 4th Int. Conf. Comput. Commun. Netw. Technol.*, Jul. 2013, pp. 1–6.

[92] M. Kumar, R. B. Pachori, and U. R. Acharya, "An efficient automated technique for CAD diagnosis using flexible analytic wavelet transform and entropy features extracted from HRV signals," *Expert Syst. Appl.*, vol. 63, pp. 165–172, Nov. 2016.

[93] W. Chen, Z. Wang, H. Xie, and W. Yu, "Characterization of surface EMG signal based on fuzzy entropy," *IEEE Trans. Neural Syst. Rehabil. Eng.*, vol. 15, no. 2, pp. 266–272, Jun. 2007.

[94] U. R. Acharya, H. Fujita, V. K. Sudarshan, S. Bhat, and J. E. Koh, "Application of entropies for automated diagnosis of epilepsy using EEG signals: A review," *Knowl. Based Syst.*, vol. 88, pp. 85–96, Nov. 2015.

[95] R. Sharma, R. Pachori, and U. Acharya, "An integrated index for the identification of focal electroencephalogram signals using discrete wavelet transform and entropy measures," *Entropy*, vol. 17, no. 12, pp. 5218–5240, Jul. 2015.

[96] L. Hussain, S. Anjum, W. Aziz, and M. M. Abbasi, "Complexity analysis of EEG Moto movement with eye open and close subjects using multiscale sample entropy (MSE) technique," *J. Ponte*, vol. 72, no. 7, pp. 1–9, Jul. 2016.

[97] L. Hussain and W. Aziz, "Time-frequency spatial wavelet phase coherence analysis of EEG in EC and EO during resting state," *Procedia Comput. Sci.*, vol. 95, pp. 297–302, Jan. 2016.

[98] A. Qumar, W. Aziz, S. Saeed, I. Ahmed, and L. Hussain, "Comparative study of multiscale entropy analysis and symbolic time series analysis when applied to human gait dynamics," in *Proc. Int. Conf. Open Source Syst. Technol. (ICOSST)*, 2013, pp. 126–132.

[99] L. Wang *et al.*, "Automatic epileptic seizure detection in EEG signals using multi-domain feature extraction and nonlinear analysis," *Entropy*, vol. 19, no. 6, p. 222, Jun. 2017.

[100] H. Azami and J. Escudero, "Improved multiscale permutation entropy for biomedical signal analysis: Interpretation and application to electroencephalogram recordings," *Biomed. Signal Process. Control*, vol. 23, pp. 28–41, Jan. 2016.

[101] M. Costa, A. L. Goldberger, and C.-K. Peng, "Multiscale entropy analysis of complex physiologic time series," *Phys. Rev. Lett.*, vol. 89, Jul. 2002, Art. no. 068102.

[102] W. Aziz and M. Arif, "Complexity analysis of stride interval time series by threshold dependent symbolic entropy," *Eur. J. Appl. Physiol.*, vol. 98, no. 1, pp. 30–40, Sep. 2006.

[103] C.-K. Peng, M. Costa, and A. L. Goldberger, "Adaptive data analysis of complex fluctuations in physiologic time series," *Adv. Adapt. Data Anal.*, vol. 1, no. 1, pp. 61–70, Jan. 2009.

[104] R. Arking and S. P. Dudas, "Review of genetic investigations into the aging processes of drosophila," *J. Amer. Geriatrics Soc.*, vol. 37, no. 8, pp. 757–773, Aug. 1989.

[105] S. Kornecki and V. Zschorlich, "The nature of the stabilizing functions of skeletal muscles," *J. Biomech.*, vol. 27, no. 2, pp. 215–225, Feb. 1994.

[106] S. Schiaffino and C. Reggiani, "Myosin isoforms in mammalian skeletal muscle," *J. Appl. Physiol.*, vol. 77, no. 2, pp. 493–501, Aug. 1994.

[107] M. F. Siddiqui, S. Rast, M. Lynn, A. P. Auchus, and R. F. Pfeiffer, "Autonomic dysfunction in Parkinson's disease: A comprehensive symptom survey," *Parkinsonism Rel. Disorders*, vol. 8, no. 4, pp. 277–284, Mar. 2002.

[108] D. E. Vaillancourt and K. M. Newell, "The dynamics of resting and postural tremor in Parkinson's disease," *Clin. Neurophysiol.*, vol. 111, no. 11, pp. 2046–2056, 2000.

[109] D. E. Vaillancourt, A. B. Slifkin, and K. M. Newell, "Regularity of force tremor in Parkinson's disease," *Clin. Neurophysiol.*, vol. 112, no. 9, pp. 1594–1603, Sep. 2001.

[110] M. D. West, "The cellular and molecular biology of skin aging," *Arch. Dermatol.*, vol. 130, no. 1, pp. 87–95, Jan. 1994.

[111] C. E. Finch and R. G. Gosden, "Animal models for the human menopause," in *Aging, Reproduction, and the Climacteric*. Boston, MA, USA: Springer, 1986, pp. 3–34.

[112] J. Y. Wei and B. J. Gersh, "Heart disease in the elderly," *Current Problems Cardiol.*, vol. 12, no. 1, pp. 7–65, Jan. 1987.

[113] P. M. Mosher-Ashley, "Procedural and methodological parameters in behavioral-gerontological research: A review," *Int. J. Aging Hum. Dev.*, vol. 24, no. 3, pp. 189–229, Apr. 1987.

[114] D. E. Vaillancourt and K. M. Newell, "Changing complexity in human behavior and physiology through aging and disease," *Neurobiol. Aging*, vol. 23, no. 1, pp. 1–11, Jan./Feb. 2002.

[115] Z. Erim, M. F. Beg, D. T. Burke, and C. J. de Luca, "Effects of aging on motor-unit control properties," *J. Neurophysiol.*, vol. 82, no. 5, pp. 2081–2091, Nov. 1999.

[116] M. E. Galganski, A. J. Fuglevand, and R. M. Enoka, "Reduced control of motor output in a human hand muscle of elderly subjects during submaximal contractions," *J. Neurophysiol.*, vol. 69, no. 6, pp. 2108–2115, Jun. 1993.

[117] D. M. Connelly, C. L. Rice, M. R. Roos, and A. A. Vandervoort, "Motor unit firing rates and contractile properties in tibialis anterior of young and old men," *J. Appl. Physiol.*, vol. 87, no. 2, pp. 843–852, Aug. 1999.

[118] M. Flück and H. Hoppeler, "Molecular basis of skeletal muscle plasticity-from gene to form and function," in *Reviews of Physiology, Biochemistry and Pharmacology*. Berlin, Germany: Springer, 2003, pp. 159–216.

[119] M. J. Thun, J. O. DeLancey, M. M. Center, A. Jemal, and E. M. Ward, "The global burden of cancer: Priorities for prevention," *Carcinogenesis*, vol. 31, no. 1, pp. 100–110, Jan. 2010.

MALIK SAJJAD AHMED NADEEM received the Ph.D. degree from the University of Paris Nord, in 2011. He is currently with the Department of Computer Sciences and Information Technology, The University of Azad Jammu and Kashmir, Muzaffarabad, as an Assistant Professor. He has published various journal papers in the area of machine learning.

LAL HUSSAIN received the M.S. degree (Hons.) in communication and networks from Iqra University, Islamabad, Pakistan, in 2012, and the Ph.D. degree from the Department of Computer Science and Information Technology, The University of Azad Jammu and Kashmir, Muzaffarabad, Pakistan, in 2016, where he is currently an Assistant Professor. He was a Visiting Ph.D. Researcher with Lancaster University, U.K., for six months, under the HEC International Research Initiative Program, and worked under the supervision of Dr. A. Stefanovska, as a Professor of biomedical physics with the Physics Department, Lancaster University, U.K. He has authored more than 20 publications of highly reputed peer-reviewed and impact fact journals. He presented various talks at Pakistan, U.K., and USA. His research interests include biomedical signal processing with concentration in complexity measures, time–frequency representation methods, cross-frequency coupling to analyze the dynamics of neurophysiological and physiological signals, neural networks, machine learning classification, regression, and prediction techniques for the detection of cancer, epilepsy, brain dynamics, and diseases (i.e., autism spectrum disorder (ASD) and attention-deficit/hyperactivity disorder (ADHD), Alzheimer's disease, and brain tumor), and image processing and segmentation.

WAJID AZIZ received the B.Sc. and M.Sc. degrees from The University of Azad Jammu and Kashmir University (UAJ&K), Muzaffarabad, Pakistan, and the Ph.D. degree from the Pakistan Institute of Engineering and Applied Sciences (PIEAS), Islamabad, Pakistan.

He started his career with UAJ&K, in 1998, as a Lecturer. He is currently a Professor with the College of Computer Science and Engineering, University of Jeddah, Jeddah, Saudi Arabia. His core research expertise is in biomedical information systems, and his focused research areas are biomedical signal processing, time-series analysis, and biomedical data analytics. He has published three books and more than 45 research articles in the reputed national and international journals and conference proceedings. Based on his academic and research contributions, he was a recipient of the HEC University Best Teacher Award for the year 2012–2013 awarded by HEC Pakistan, in 2014, and the University Best Teacher Award by UAJ&K, in 2013.

ISHTIAQ RASOOL KHAN received the B.Sc. degree in electrical engineering from the University of Engineering and Technology, Taxila, Pakistan, in 1992, the M.S. degree in systems engineering from Quaid-i-Azam University, Islamabad, Pakistan, in 1994, and the M.S. degree in information engineering and the Ph.D. degree in digital signal processing from Hokkaido University, Japan, in 1998 and 2000, respectively. He was a JSPS Fellow with Hokkaido University, Japan, from 2000 to 2002. He was with the University of Kitakyushu, Japan, the Kyushu Institute of Technology, Japan, and the Institute for Infocomm Research, A*STAR, Singapore. He is currently a Professor with the College of Computer Science and Engineering, University of Jeddah. His research interests include high dynamic range imaging, data analytics, and digital signal processing.

ABDULRAHMAN A. ALSHDADI received the Ph.D. degree in cloud computing from the University of Southampton, Southampton, U.K., in 2018. He is currently an Assistant Professor of computer science with the College of Computer Science and Engineering Technology, University of Jeddah, Jeddah, Saudi Arabia, where he is also the Head of the Computer Science and Artificial Intelligent Department (CSAI) and the Vice Dean of the College of Computer Science and Engineering (CCSE). He has published numerous conference papers, journal papers, and one book chapter. His research interests span mainly around Industry 4.0 prestaining issues of cloud computing and fog computing security, the Internet of Things (IoT) and smart cities, intelligent systems, deep learning, data science analytics, and modeling.

QURAT-UL-AIN CHAUDHRY received the B.S. and M.Phil. degrees in computer science from the Department of Computer Science and IT, The University of Azad Jammu and Kashmir, Muzaffarabad, in 2015 and 2018, respectively, where she is currently a Visiting Lecturer with the Department of Computer Science and IT. Her research interest includes biomedical image processing and analysis.

• • •